Fibre optic sensors for delamination identification in composite beams using a genetic algorithm

Hang-yin Ling[1,3], Kin-tak Lau[1], Li Cheng[1] and Wei Jin[2]

[1] Department of Mechanical Engineering, The Hong Kong Polytechnic University, Hong Kong, People's Republic of China
[2] Department of Electrical Engineering, The Hong Kong Polytechnic University, Hong Kong, People's Republic of China

E-mail: carrie.lhy@polyu.edu.hk

Abstract
Fibre Bragg grating (FBG) sensors associated with a genetic algorithm (GA) were used to detect and identify the size and location of delaminations in composite beams. A theoretical beam model is implemented into the GA for on-line delamination parameter searching. The objective function of this vibration-based delamination detection problem in the GA is defined as the sum of squared ratios of the differences between the shifts of eigenvalues of a delaminated beam measured by the FBG sensors and calculated from the theoretical beam model to the eigenvalues of an intact beam measured by the FBG sensors in the first three vibration modes. The principle of the FBG sensors for vibration detection is briefly discussed in this paper. A laser vibrometer and an accelerometer are utilized to compare the results measured from the FBG sensors. The reliability of using the FBG sensors for delamination detection is highlighted. Different delamination sizes and locations in spanwise and thickness-wise directions of the beams are simulated to demonstrate the feasibility of using the GA for the detection of delamination in the composite beams.

(Some figures in this article are in colour only in the electronic version)

1. Introduction

In the past decade, fibre-reinforced polymer composites have been widely used in aerospace and civil engineering applications due to their high specific strength to weight ratio and excellent corrosion resistance. Delamination, which is a kind of characterized damage only found in the composites because of the lack of reinforcement in the through-the-thickness direction, is readily caused by low energy impact as well as fatigue loading in the in-service condition. As the delamination of structures cannot be detected visually, conventional non-destructive evaluation (NDT) techniques such as the x-ray, thermography, eddy current and ultrasonic C-scan methods have been utilized for delamination detection.

However, these techniques are not only time-consuming, costly and requiring direct human accessibility of structures, but also involve a restriction on static measurement which means that they cannot provide real-time structural health monitoring of the condition of the structures. Therefore, smart structure technology has been attracting much interest with a view to the achievement of continuous and *in situ* monitoring of composite structures, due to its ability to provide on-line damage detection for identifying the damage location as well as examining the severity of the structures using sensor information. Recently, fibre optic sensors have been broadly accepted as strain-measuring devices that can be integrated into the composite structures to form smart composites. Zhou and Sim [1] have provided a comprehensive review on damage detection and assessment in composite structures utilizing embedded fibre optic sensors. They have pointed out that

---

[3] Author to whom any correspondence should be addressed.

the embedded fibre optic sensors can experience the same strain gradient as damaged structures. Intensity-modulated, interferometric, extrinsic Fabry–Perot interferometric (EFPI), fibre Bragg grating (FBG) and polarimetric sensors are the most popular kinds of fibre optic sensors used for damage detection [1].

Elvin and Leung [2] demonstrated the feasibility of using an embedded Mach–Zehnder interferometer sensor for delamination detection. However, they only detected the presence of delamination and could not identify delamination size and location. Moreover, EFPI sensors have been proposed for real-time monitoring of edge-induced and internal delamination in composites [3], but again the delamination size and location could not be determined. A later work reported by Sanders *et al* [4] established that the delamination size and location for composite beams could be identified by measuring the change of the first five modal frequencies by using EFPI fibre optic sensors combined with a feed-forward back-propagation neural network. The trained neural network always overestimates the delamination size and location with an average error of 5%, approximately. However, only the delamination along the spanwise direction could be found.

Owing to the disadvantages of EFPI fibre optic sensors such as stress concentrations around the sensors and the difficulty of developing a serial quasi-distributed sensor network, the FBG sensors are preferable for use for delamination detection by means of both static and dynamic strain measurements because of their multiplexing characteristics. In a three-point bending test, Leng and Asundi [5] employed a FBG sensor for the inspection of delamination in composite laminates as well as cracks of aluminum plates. They clearly observed that the flexural strain of damaged structures was much higher compared with that of an undamaged structure subjected to static loading. Ling *et al* [6] demonstrated experimentally that measurements of the natural frequencies of a glass fibre composite beam by a FBG sensor and a laser vibrometer could give comparable results. The existence of delamination could be identified by utilizing the FBG sensors. Recently, Takeda *et al* [7] have revealed that small-diameter FBG sensors could be applied for the detection of edge delamination in carbon fibre reinforced plastic quasi-isotropic laminates under cyclic loading conditions. They claimed that the edge delamination could be quantitatively determined by monitoring the reflection spectrum of the small-diameter FBG sensor.

As the damage detection is an inverse engineering problem, it is difficult to identify the damage directly from the raw data from the fibre optic sensors. The mapping relationship between the structural damage feature proxy and the practical damage status can be established using a genetic algorithm (GA) or artificial neural network (ANN). A neural network has been coupled with fibre optic sensors to identify damage with a trained ANN using a set of known parameters of structures [4]. As compared with the ANN, the GA searches from a population of points in the region of the whole solution space, rather than a single point, and can obtain the global optimum. Easy implementation is another advantage of the GA, because only an objective function is required and other information is not necessary. Many researchers have demonstrated the potential of using GAs for damage

detection [8–13]. Yang *et al* [12] used a surface bonded interferometric optical fibre to extract the integral strain for detection of a three-dimensional crack in plates, in which the detection procedure was similar to the Elvin and Leung [2] one, with a GA. They successfully showed the feasibility of using this detection method to establish crack size and location, as illustrated by a number of different examples based on a FEM model. Identification of delaminations in composite beams using spectral estimation and a GA has been presented by Nag *et al* [13]. However, research up to this point has not been focused on the utilization of embedded FBG sensors associated with a GA for the detection of delamination.

In this paper, a GA is applied in identification of delamination in composite beams by minimizing an objective function. The objective function directly compares with the changes in natural frequencies of the delaminated beams measured using embedded FBG sensors and calculated using a theoretical constrained beam model [14]. The principle of vibration sensing with the FBG sensors is discussed. The reliability of the FBG sensors for vibration monitoring is compared with those of a laser vibrometer and a piezoelectric accelerometer. The theoretical constrained beam model was implemented into the GA to search for the best delamination parameters. A number of examples with different delamination parameters are then used to demonstrate the feasibility of the present damage detection method.

2. Fibre Bragg grating sensors

The principle of the FBG strain sensor is measuring the change of the reflected signal from a grating when it is subjected to elongation. This change would influence the reflective index (n_b) and spatial pitch (Λ) at the core of the sensor [15]. A schematic illustration of the FBG system used for strain measurement is shown in figure 1.

To utilize the FBG sensor for the strain measurement, a grating, which acts essentially as a wavelength selective mirror, must be first written in the core of an optical fibre. The grating was written by exposing the fibre to a pair of strong ultra-violet (UV) interference signals. This method of grating writing for strain and temperature measurements is called the 'phase mask technique'. According to Bragg's law, the Bragg wavelength (λ_B) that is reflected from the sensor is given by

$$\lambda_B = 2n_b\Lambda. \tag{1}$$

As any changes of strain in the grating region result in change of the spatial period and core refractive index, the mechanical strain (ε_g) is determined by the measurement of the Bragg wavelength shift ($\Delta\lambda_B$) [16]. Neglecting the temperature effect on the sensor and the strain transfer to the fibre in the transverse direction, the change of the Bragg wavelength shift can be expressed as

$$\Delta\lambda_B = K\varepsilon_g \tag{2}$$

where K is called the 'theoretical gauge constant' [17], which can be determined experimentally. In general, $\Delta\lambda_B$ can be obtained using an optical spectrum analyser (OSA). However, the OSA cannot be used to measure $\Delta\lambda_B$ dynamically. To solve this problem, the new linear relationship between the
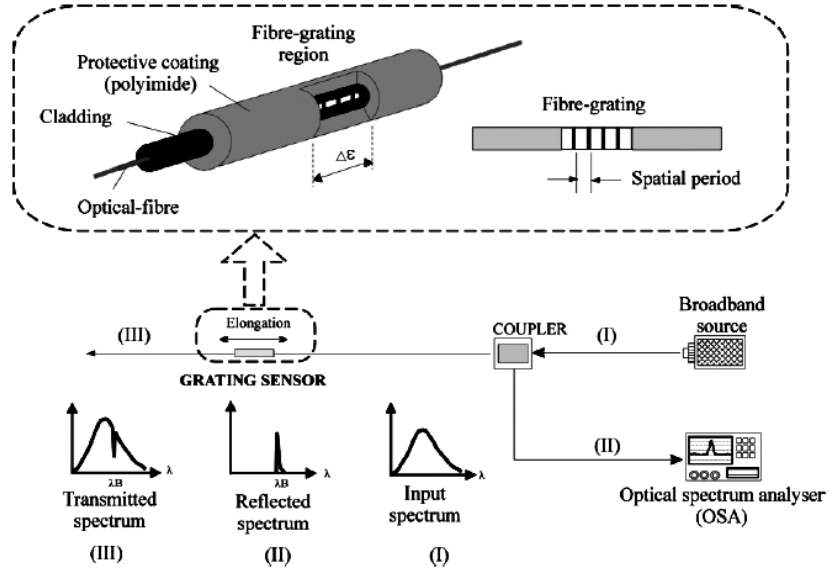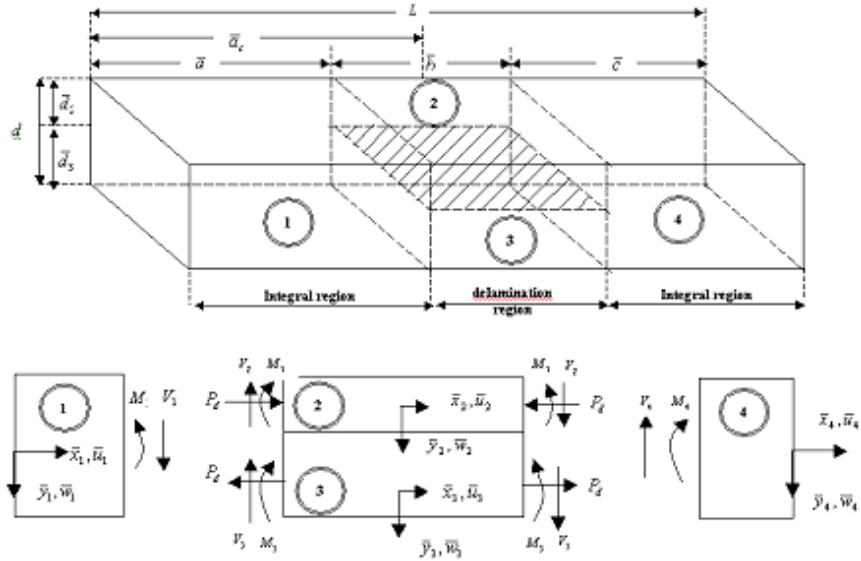
Figure 1. The FBG strain-measuring system.

Figure 2. A constrained beam model.

photovoltage variation (ΔV_{photo}) that is measured in real time by the photodetector and $\Delta\lambda_B$ is introduced as follows:

$$\Delta V_{\text{photo}} = C\Delta\lambda_B \tag{3}$$

where C is the proportion constant which depends on the system desired. By combining equations (2) and (3), the following equation is formed:

$$\Delta V_{\text{photo}} = S\Delta\varepsilon_g \tag{4}$$

where $S = CK$. It is recalled that the photovoltage variation is related to the power of superluminescent light emitting diodes (SLED) and to the power losses due to factors such as the reflectivity of the grating, the splice loss of the fibre, the insertion loss of the optical tunable filter (OTF) and the power splitting reduction through the coupler, for the above FBG measurement set-up. A signal analyser was used in the experiments to detect the photovoltage variation, so the dynamic strain of the structures can be shown by the signal analyser in the time domain. The natural frequencies of the structures can also be obtained by using the frequency response function.

3. Theoretical modeling of vibration in a delaminated beam

In this paper, a constrained beam model with an arbitrarily located through-width delamination, as shown in figure 2, developed by Mujumdar and Suryanarayan [14] was used to simulate delaminated composite beams. This constrained beam model consists of four beam segments. Each beam segment was treated as an Euler beam, for which we need not consider the shear distortion, and the aspect ratio (length to thickness ratio) of the beam is equal to or larger than 10,
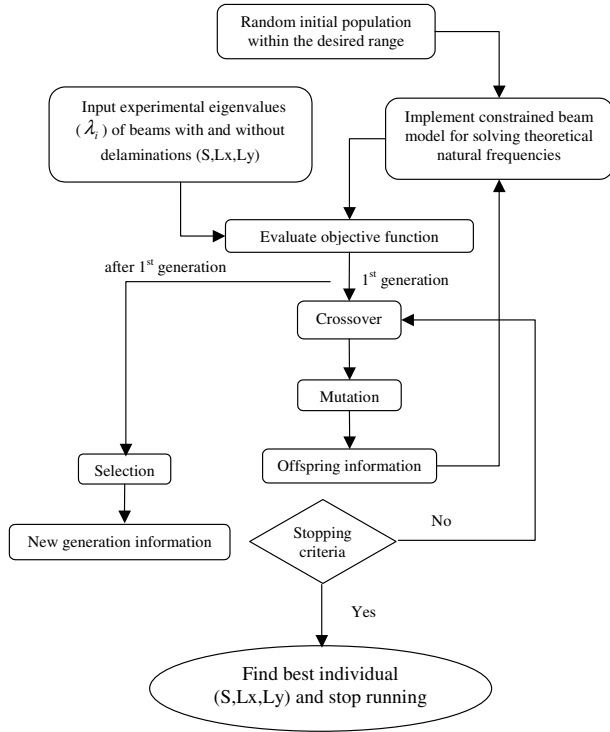
289

Figure 3. An overview of the genetic algorithm searching method.

for vibration analysis. In this model, the beams were assumed to be homogeneous and isotropic. For the sake of simplicity, only a single delamination was considered in this study. Also, it was assumed that there is no gap between the layers in the delamination region under all conditions.

The governing equations for the transverse equilibrium for integral segments can be written in a dimensionless form as

$$\frac{\partial^4 \bar{w}_i}{\partial \bar{x}_i^4} + \left(\frac{\rho A L^4}{EI} \right) \frac{\partial^2 \bar{w}_i}{\partial t^2} = 0, \qquad i = 1, 4 \qquad (5)$$

where $\bar{x}_i = x_i/L$ and $\bar{w}_i = w_i/d$ are the dimensionless axial coordinate and the transverse displacement of the ith segment, respectively. For the delaminated segments, the governing equations can be written as

$$-EI_2 \frac{\partial^4 \bar{w}_2}{\partial \bar{x}_2^4} - P_d \frac{\partial^2 \bar{w}_2}{\partial \bar{x}_2^2} - \rho A_2 \frac{\partial^2 \bar{w}_2}{\partial t^2} - p = 0,$$

for segment 2 (6)

$$-EI_3 \frac{\partial^4 \bar{w}_3}{\partial \bar{x}_3^4} + P_d \frac{\partial^2 \bar{w}_3}{\partial \bar{x}_3^2} - \rho A_3 \frac{\partial^2 \bar{w}_3}{\partial t^2} + p = 0,$$

for segment 3 (7)

where p is the distribution of normal contact pressure between the two segments and P_d is the magnitude of the axial load in each segment.

As the axial load P_d depends on the amplitude and mode of the deformation, the second terms on the left-hand side in equations (6) and (7) are non-linear. On the basis of the free mode of deformation assumption, the non-linear terms are not taken into account. Also, in the constrained model, w_2 is assumed to be equal to w_3 everywhere in the delamination region and x_2 is equal to x_3. As a result, equations (6) and (7) can be combined to represent the behaviour of the
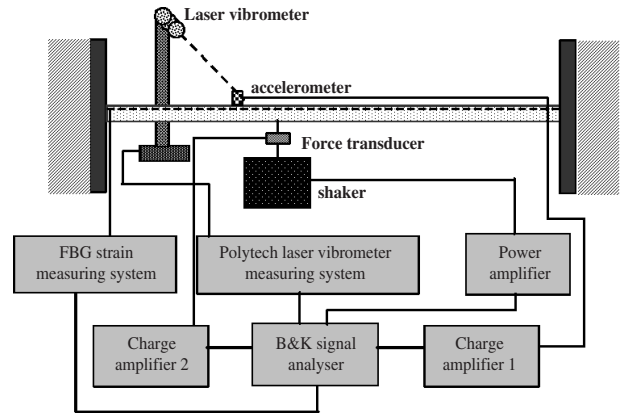
Figure 4. An experiment set-up used for the measurement of natural frequencies of beams with and without delamination using FBG sensors, a laser vibrometer and an accelerometer.

delaminated region and the equation, in dimensionless form, can be expressed as

$$\frac{\partial^4 \bar{w}_2}{\partial \bar{x}_2^4} + \left(\frac{\rho (A_2 + A_3) L^4}{E(I_2 + I_3)} \right) \frac{\partial^2 \bar{w}_2}{\partial t^2} = 0. \qquad (8)$$

The general solutions of equations (5) and (8) can be written in the following form:

$$\bar{w}_i(\bar{x}_i) = F_i C_i \qquad (9)$$

where $F_i = [\, f_{1i}(\bar{x}_i) \quad f_{2i}(\bar{x}_i) \quad f_{3i}(\bar{x}_i) \quad f_{4i}(\bar{x}_i) \,]$, $C_i = [\, c_{1i} \quad c_{2i} \quad c_{3i} \quad c_{4i} \,]^{\mathrm{T}}$ in which

$$f_{1i}(x_i) = \sin(\lambda_i \bar{x}_i), \qquad f_{2i}(x_i) = \cos(\lambda_i \bar{x}_i),$$

$$f_{3i}(x_i) = \sinh(\lambda_i \bar{x}_i) \qquad \text{and} \qquad f_{4i}(x_i) = \cosh(\lambda_i \bar{x}_i)$$

C_i is a constant matrix

where the dimensionless frequency parameters, λ_i, are given by

$$\lambda_1^4 = \lambda_4^4 = \lambda^4 = \rho A \omega^2 L^4 / EI$$

$$\lambda_2^4 = \rho (A_2 + A_3) \omega^2 L^4 / E\{I_2 + I_3\} = \lambda^4 / (\bar{d}_2^3 + \bar{d}_3^3)$$

in which $\bar{d}_2 = d_2/d$ and $\bar{d}_3 = d_3/d$.

To evaluate the natural frequencies of the delaminated beams with different clamping conditions, appropriate boundary conditions and continuity equations have to be applied at both ends and the junctions between the integral and delaminated segments respectively. The detail of the derivation of the boundary conditions and the continuity equations can be found in [14]. As a result, there is a set of 12 simultaneous linear homogeneous algebraic equations in 12 unknown constants of the continuity and boundary conditions. The frequencies can be calculated as the eigenvalues (λ_i) of this equation set.

4. The genetic algorithm for delamination identification

As the identification of delamination is an inverse problem, a search method is essential for identifying the delamination
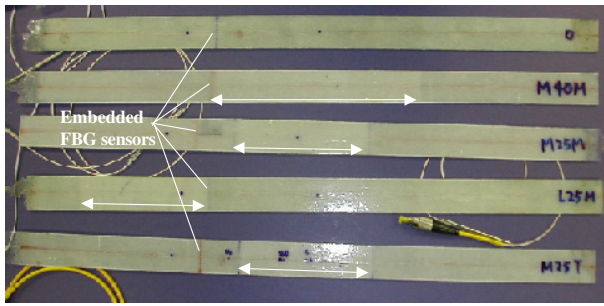
Figure 5. Glass fibre composite beams with embedded FBG sensors for various sizes and locations of delamination.

by extraction of information from embedded FBG sensors. A GA was employed in the present study in order to identify the delamination size and location for composite beams at the first three natural frequencies measured by the sensors.

The objective function of this vibration-based delamination detection problem in the GA was defined as the sum of the squared ratios of the differences between the shifts of eigenvalues of the delaminated beam measured by the sensors and calculated from a theoretical beam model to the eigenvalues of the intact beam measured by the sensors at the first three vibration modes, which can be expressed as

$$J(S, L_x, L_y) = \sum_{i=1}^{3} \left(\frac{(\lambda_{m0}^i - \lambda_m^i) - (\lambda_{t0}^i - \lambda_t^i)}{\lambda_{m0}^i} \right)^2 \quad (10)$$

where λ_m^i and λ_{m0}^i are the eigenvalues of the beams with and without delamination measured by the sensors for the ith vibration mode respectively. Similarly, λ_t^i and λ_{t0}^i are the eigenvalues of the beams with and without delamination calculated by the constrained beam model for the ith vibration mode respectively. Also, S, L_x and L_y represent the delamination size and delamination location in spanwise and thickness-wise directions respectively.

By using the GA, the best delamination parameters of the beam can be experimentally identified by minimizing the above objective function in this analysis. Firstly, initial populations that represent the delamination parameters are randomly selected within the desired range from 0 to 1. By substituting the populations (delamination parameters) into the constrained beam model, the corresponding theoretical eigenvalues of the beams can be calculated. The objective function can be evaluated by substituting in the experimental eigenvalues of the beams measured by the sensors. The individuals in the next generation are generated according to the fitness of the individuals in the previous generation. During the searching process, not only are the individuals in each generation created randomly, but also the best individual in each generation can be inherited by the next generation. After crossover and mutation in the population, the offspring is found. The offspring information is then used to calculate the eigenvalues of the beams again and the new information in the next generation is obtained. The delamination parameters are finally found in the last generation. An overview of the GA derived in this study is presented schematically in figure 3. Other standard terminologies and the basic framework of the GA can be found in [18]. 40 populations and 10 genes in each chromosome were chosen in the present study.
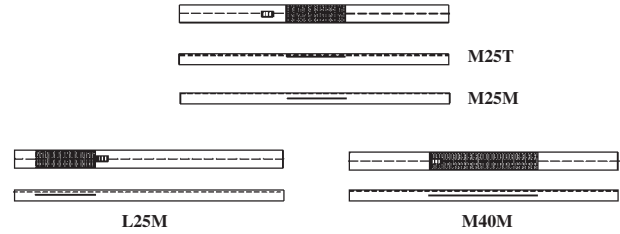

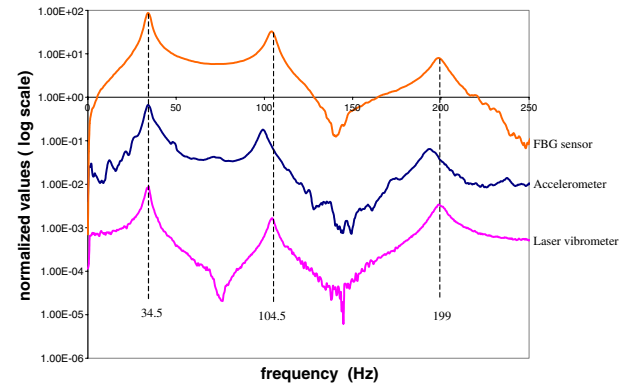**Figure 6.** Top and side views of the testing specimens.

Figure 7. The frequency response function of an intact beam obtained by a FBG sensor, an accelerometer and a laser vibrometer.

5. Experiments

An experiment set-up shown in figure 4 was employed to determine the first three natural frequencies of glass fibre composite beams with and without delamination. The beams were fixed at both ends and actuated by an electrically driven shaker with random signals. A FBG sensor was embedded into a beam during the fabrication process, located 12 cm from the right-hand end of the beam, to measure its natural frequencies. To show the reliability of utilizing the sensors for measurement of the natural frequency of the beams, an accelerometer and a laser vibrometer were used to provide a comparison. The accelerometer and the measurement point of the laser vibrometer were bonded and pointed towards the surface of the beam at the position where the sensor was embedded, respectively. In order to avoid mass effects of the accelerometer, the accelerometer was removed from the beam surface when the FBG sensor and the laser vibrometer measurements were carried out. To further investigate the influence of natural frequencies of the beam due to the mass of the accelerometer, the accelerometer was attached on the surface of the beam to measure the beam's natural frequency. The natural frequencies of the beams were directly obtained by observing the frequency response function, obtained as the ratio of the sensor output and force transducer response, in a B&K analyser unit.

Ten layers of balanced-type woven glass fibre composite laminates with a stacking sequence of $[0°]_{10}$ were fabricated by a hand lay-up process. The mechanical properties are $E_{11} = E_{22} = 13.363$ GPa, $G_{12} = 5.86$ GPa, $\nu = 0.14$ and $\rho = 1664.03$ kg m^{-3}. To simulate the delamination that has taken place, Teflon films were inserted between the glass fibre laminas during the fabrication process. Rectangular specimens with dimensions of 0.44 m × 0.025 m × 0.002 m

Figure 8. (a) The objective function in the genetic algorithm against the generation in the case of M40M; (b) delamination parameters against the generation in the case of M40M (——, the delamination location in the thickness-wise direction; ······, the delamination location in the spanwise direction; - - - -, the delamination size).
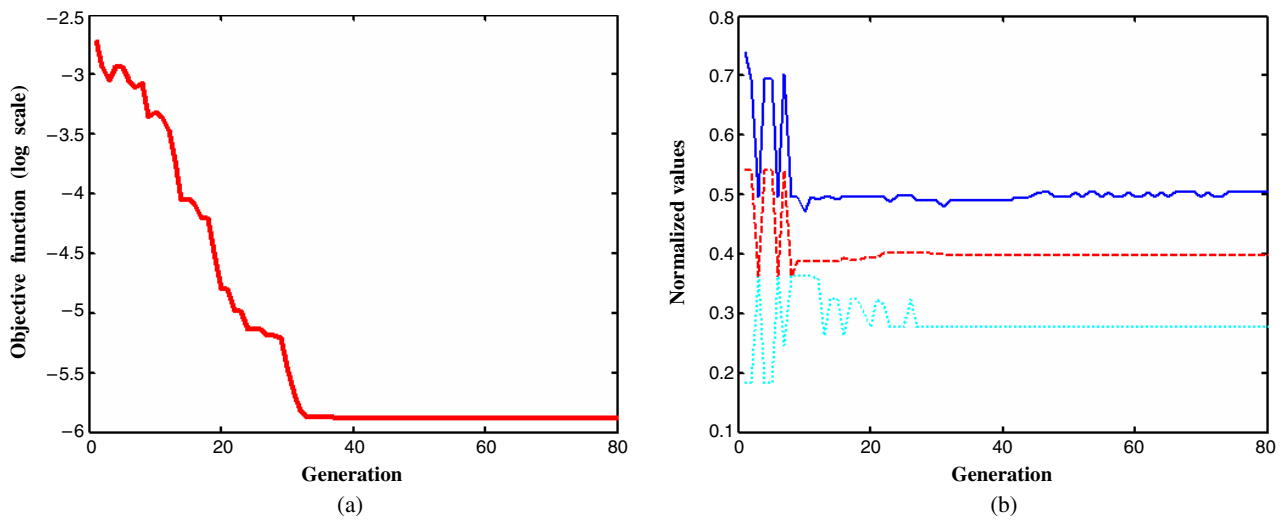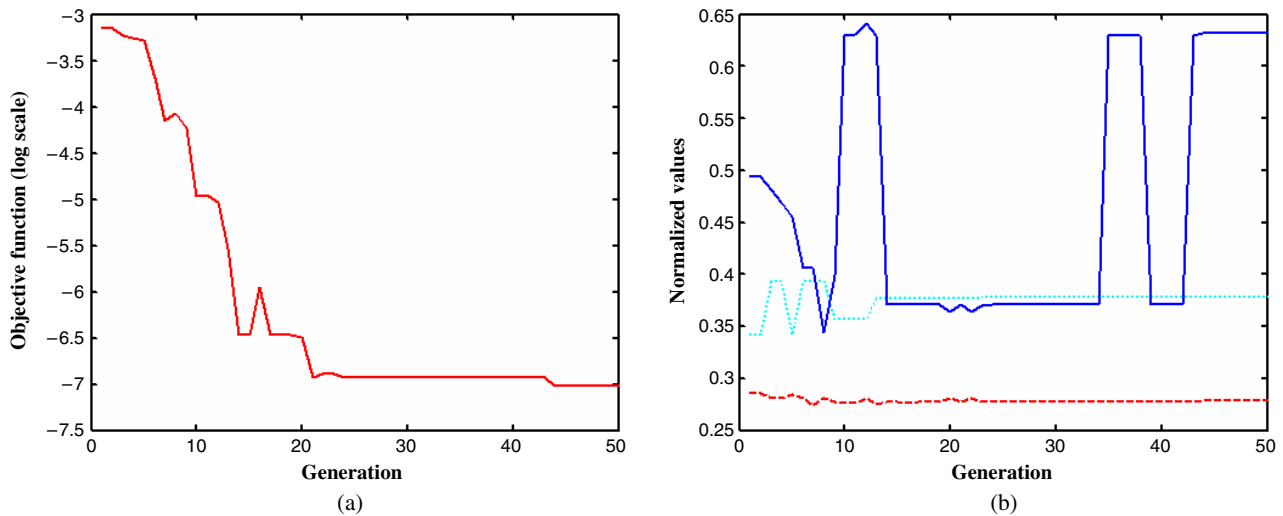

Figure 9. (a) The objective function in the genetic algorithm against the generation in the case of M25M; (b) delamination parameters against the generation in the case of M25M (——, the delamination location in the thickness-wise direction; ······, the delamination location in the spanwise direction; - - - -, the delamination size).

Table 1. The experimental results on natural frequencies of the beam with and without 25% delamination measured using the accelerometer, laser vibrometer and FBG sensor.

Sensors	Natural frequency of beam without delamination (Hz)			Natural frequency of beam with 25% delamination (L25M) (Hz)		
	Mode 1	Mode 2	Mode 3	Mode 1	Mode 2	Mode 3
Accelerometer	34.5	101.5	198.5	35.5	95	200
Laser vibrometer	34.5	104.5	199	34.5	93	196.5
FBG sensor	34.5	104.5	199	34.5	93	196.5

were cut from the composite laminates. As the embedding of the Teflon films might affect the natural frequency of the beams, removal of the Teflon films after the process of curing the composite is necessary. Open-mode vibration may occur due to the effect of through-width delamination. In the present study, we focus on the effects on the delaminated beam in the vibration without considering the open-mode vibration. The

vibration amplitude was kept as small as possible to avoid open-mode vibration. All specimens are photographically and schematically shown in figures 5 and 6. It is noted that both M25T and M25M had 25% delaminations at the mid-span, located at the interface between the eighth and ninth layers and the mid-plane of the beam, respectively. In the case of L25M, a 25% delamination prescribed at 0.07 m was measured
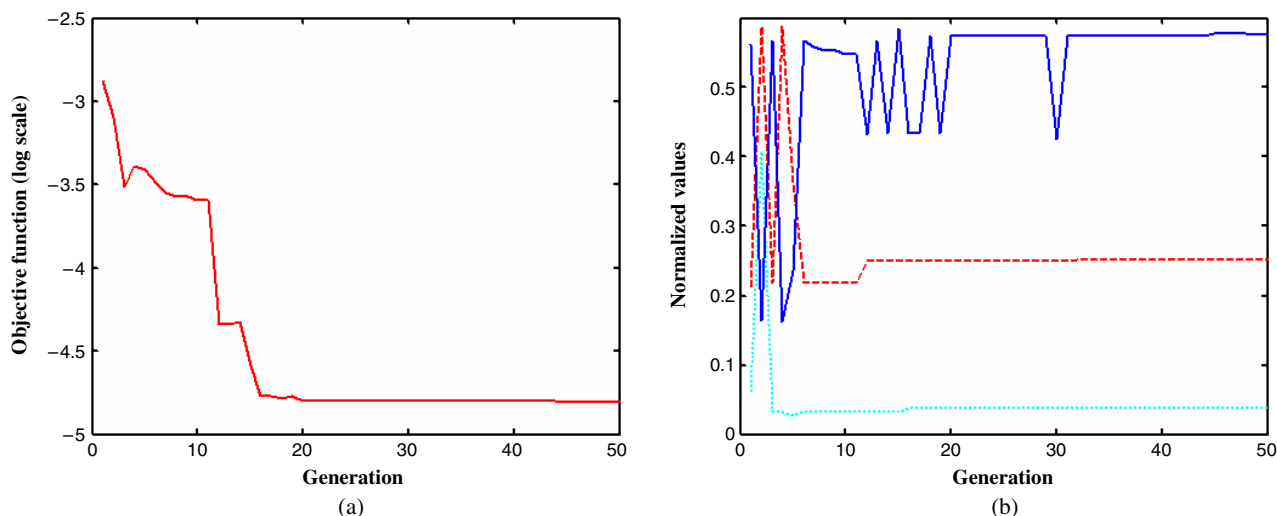
Figure 10. (a) The objective function in the genetic algorithm against the generation in the case of L25M; (b) delamination parameters against the generation in the case of L25M (——, the delamination location in the thickness-wise direction; · · · · · ·, the delamination location in the spanwise direction; - - - -, the delamination size).
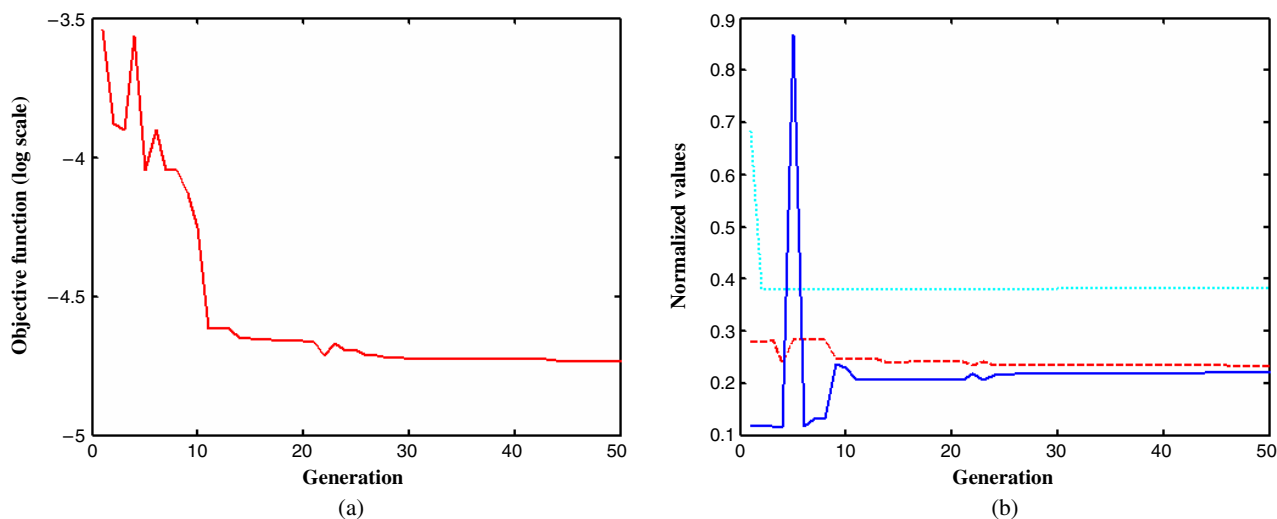

Figure 11. (a) The objective function in the genetic algorithm against the generation in the case of M25T; (b) delamination parameters against the generation in the case of M25T (——, the delamination location in the thickness-wise direction; · · · · · ·, the delamination location in the spanwise direction; - - - -, the delamination size).

from the left and located at the mid-plane of the beam. M40M presents a 40% delamination that was located at the mid-span and mid-plane of the beam.

6. Experimental results and discussion

The frequency response function of a clamped–clamped intact beam is plotted in figure 7. It was obvious that a good agreement of the results obtained from the FBG sensor and a laser vibrometer was demonstrated. However, mismatch of the accelerometer and the laser vibrometer is indicated. This inconsistent result might be due to the mass effect of the accelerometer.

The FBG sensor and the laser vibrometer measured the natural frequencies of the beam with 25% delamination as reduced. This demonstrated that the FBG sensor could be used to detect the existence of the delamination by comparing the natural frequencies of the delaminated beam and the intact one. However, it was found that the natural frequencies measured using the accelerometer for the delaminated beam were slightly increased at the first and third modes and decreased at the second mode, as shown in table 1. The reason is that the mass effect of the accelerometer dominated the delamination effect on the natural frequencies at the first and third modes, so the natural frequencies of the delaminated beam increased. As the accelerometer was located at a position near the nodal point of mode 2, its mass effect on the natural frequency of the delaminated beam is insignificant. Consequently, the delamination effect on the natural frequency is normally shown at the second mode. From the comparison, it appears that the FBG sensor would be the most suitable device among these three vibration monitoring devices for making *in situ*

Table 2. Experimental and theoretical modal eigenvalues for beams with various delamination sizes and locations.

Case	Mode number	Experimental eigenvalues	Theoretical eigenvalues	Difference between experimental and theoretical results (%)
0	1	4.45	4.73	5.92
	2	7.49	7.85	4.59
	3	10.80	10.99	1.73
L25M	1	4.17	4.45	6.29
	2	6.93	7.28	4.81
	3	10.31	10.51	1.90
M25T	1	4.44	4.73	6.13
	2	7.26	7.64	4.97
	3	10.78	10.92	1.28
M25M	1	4.41	4.72	6.57
	2	6.16	7.24	14.92
	3	9.50	10.73	11.46
M40M	1	4.38	4.67	6.21
	2	6.59	6.63	0.60
	3	9.73	9.67	0.62

Table 3. Predicted and actual delamination sizes and locations of beams in different cases.

Case	L25M	M25T	M25M	M40M
Actual delamination size (% of total beam length)	0.2500	0.2500	0.2500	0.4000
Predicted delamination size (% of total beam length)	0.2512	0.2327	0.2786	0.3988
Percentage difference (%)	0.48	6.92	11.44	0.3
Actual delamination location in spanwise direction (% of total beam length from left)	0.0500	0.3750	0.3750	0.3000
Predicted delamination location in spanwise direction (% of total beam length from left)	0.0371	0.3822	0.3783	0.2776
Percentage difference (%)	25.8	1.92	0.88	7.47
Actual delamination location in thickness-wise direction (% of beam thickness from top)	0.5000	0.2000	0.5000	0.5000
Predicted delamination location in thickness-wise direction (% of beam thickness from top)	0.5758	0.2239	0.6325	0.5034
Percentage difference (%)	15.16	11.95	26.5	0.68

measurements of the shift of the natural frequency of the delaminated beams.

Experimental eigenvalues measured using the FBG sensors agreed well with theoretical eigenvalues calculated from a constrained beam model, as shown in table 2. Reduction of the eigenvalues was noticed, as the delamination existed in all cases. The percentage difference between the experimental and theoretical results decreased for the higher modes, except in the case of M25M.

The convergence of an objective function and the delamination parameters with increasing generation number in various cases is illustrated in figures 8–11. In these figures, it is observed that the GA correctly locates the delamination and its size after no more than 50 generations in all cases. Table 3 lists the predicted delamination sizes and locations for the beams obtained using the GA in different cases and the corresponding percentage differences. In all cases, the percentage difference between the predicted and the actual value of the delamination location in the thickness-wise direction is higher than that between the predicted and the actual value of the delamination size and location in the spanwise direction. In the GA search for the thickness-wise location for the delamination based on the theoretical constrained beam model, all of the normalized values from 0 to 1 are possible answers. However, we know that the delamination only occurs between the plies of the composite laminates in a real situation. For a ten-ply composite laminate, there are only 11 possible values for thickness-wise delamination location in the range between 0 and 1, with 0.1 intervals. Unrealizable results would be generated in the GA program and the inaccurately predicted values would then be obtained as results of the prediction errors for the delamination location in the thickness-wise direction. Modification of the delaminated beam model based on classical laminate theory would be useful for minimizing this difference. Integer encoding would also be effective for giving some constraints on the search process of the GA for calculating the theoretical eigenvalues. Around 25% difference between the predicted and actual values of the delamination location in the spanwise direction in the case of L25M is also noted in table 3. This large difference could be explained by the effect of clamping

on the delaminated beam, as the delamination of the beam was located only 2 cm from the clamped end.

7. Conclusion

A GA based on measurements from embedded FBG sensors has successfully predicted some delamination parameters (sizes, locations in spanwise and thickness-wise directions) in composite beams concurrently. By using this method, only the measuring information from the first three vibration modes of the beams is needed to detect and identify the delamination size and location for the beams. The FBG sensors showed comparable results to a laser vibrometer when measuring the natural frequency of the beam. However, the use of an accelerometer generated measurement errors because of the mass penalty. It was revealed that FBG sensors would be more suitable for real-time monitoring of composite structures owing to their embeddability and low weight. Extensive work will concentrate on the effects of the mode number and an objective function, with combination of the mode shape and natural frequency, on the accuracy of the detection of delamination in composite structures in the future.

References

[1] Zhou G and Sim L M 2002 Damage detection and assessment in fibre-reinforced composite structures with embedded fibre optic sensors—review *Smart Mater. Struct.* **11** 925–39

[2] Elvin N and Leung C K Y 1997 Feasibility of delamination detection with embedded optical fibers *Proc. SPIE* **3041** 627–34

[3] Bhatia V, Schmid C A, Murphy K A, Claus R O, Tran T A, Greene J A and Miller M S 1995 Optical fiber sensing technique for edge-induced and internal delamination detection in composites *Smart Mater. Struct.* **4** 164–9

[4] Watkins S E, Sanders G W, Akhavan F and Chandrashekhara K 2002 Modal analysis using fibre optic sensors and neural networks for prediction of composite beam delamination *Smart Mater. Struct.* **11** 489–95

[5] Leng J S and Asundi A 2002 Non-destructive evaluation of smart materials by using extrinsic Fabry–Perot interferometric and fibre Bragg grating sensors *NDT&E Int.* **35** 273–6

[6] Ling H Y, Lau K T and Li C 2004 Determination of dynamic stress profile and delamination detection of composite structures using embedded multiplexed fibre-optic sensors *Compos. Struct.* **66** 317–26

[7] Takeda S, Okabe Y, Yamamoto T and Takeda N 2003 Detection of edge delamination in CFRP laminates under cyclic loading using small-diameter FBG sensors *Compos. Sci. Technol.* **63** 1885–94

[8] Hao H, Asce M and Xia Y 2002 Vibration-based damage detection of structures by genetic algorithm *J. Comput. Civil Eng.* **16** 222–9

[9] Krawczuk M and Ostachowicz W 2002 Identification of delamination in composite beams by genetic algorithm *Sci. Eng. Compos. Mater.* **10** 147–55

[10] Friswell M I, Penny J E T and Garvey S D 1998 A combined genetic and eigensensitivity algorithm for the location of damage in structures *Comput. Struct.* **69** 547–56

[11] Krawczuk M 2002 Application of spectral beam finite element with a crack and iterative search technique for damage detection *Finite Elem. Anal. Des.* **38** 537–48

[12] Yang Z L, Liu G R and Lam K Y 2002 An inverse procedure for crack detection using integral strain measured by optical fibers *Smart Mater. Struct.* **11** 72–8

[13] Nag A, Mahapatra D R and Gopalakrishnan S 2002 Identification of delamination in composite beams using spectral estimation and a genetic algorithm *Smart Mater. Struct.* **11** 899–908

[14] Mujumdar P M and Suryanarayan S 1988 Flexural vibrations of beams with delaminations *J. Sound Vib.* **125** 441–61

[15] Lau K T 2003 Fibre-optic sensors and smart composites for concrete applications: a review article *Mag. Concr. Res.* **55** 19–34

[16] Maaskant R, Alavie T, Measures R M, Tadros G, Rizkalla S H and Guhathakurta A 1997 Fibre-optic Bragg grating sensor for bridge monitoring *J. Cement Concrete Compos.* **19** 21–33

[17] Saouma V E, Anderson D Z, Ostrander K, Lee B and Slowik V 1998 Application of fibre Bragg grating in local and remote infrastructure health monitoring *J. Mater. Struct.* **31** 259–66

[18] Goldberg D E 1989 *Genetic Algorithm in Search, Optimization, and Machine Learning* (Reading, MA: Addison-Wesley)